Annual Review of Fluid Mechanics

Bubble Dynamics in Soft and Biological Matter

Benjamin Dollet,[1] Philippe Marmottant,[1] and Valeria Garbin[2]

[1]LIPhy (Laboratoire Interdisciplinaire de Physique), Université Grenoble Alpes, CNRS, 38400 Saint-Martin-d'Hères, France

[2]Department of Chemical Engineering, Imperial College London, London SW7 2AZ, United Kingdom; email: v.garbin@imperial.ac.uk

Annu. Rev. Fluid Mech. 2019. 51:331–55

First published as a Review in Advance on September 19, 2018

The *Annual Review of Fluid Mechanics* is online at fluid.annualreviews.org

https://doi.org/10.1146/annurev-fluid-010518-040352

Keywords

bubbles, cavitation, viscoelasticity, rheology, acoustics, resonance

Abstract

Bubbles are present in a large variety of emerging applications, from advanced materials to biology and medicine, as either laser-generated or acoustically driven bubbles. In these applications, the bubbles undergo oscillatory dynamics and collapse inside—or near—soft and biological materials. The presence of a soft, viscoelastic medium strongly affects the bubble dynamics, both its linear resonance properties and its nonlinear behavior. Surfactant molecules or solid particles adsorbed on a bubble surface can also modify the bubble dynamics through the rheological properties of the interfacial layer. Furthermore, the interaction of bubbles with biological cells and tissues is highly dependent on the mechanical properties of these soft deformable media. This review covers recent developments in bubble dynamics in soft and biological matter for different confinement conditions: bubbles in a viscoelastic medium, coated by a viscoelastic layer, or in the vicinity of soft confinement or objects. The review surveys current work in the field and illustrates open questions for future research.

1. INTRODUCTION

Gas bubble: the bubble contains a permanent, noncondensable gas

Vapor bubble: the bubble contains the vapor of the surrounding liquid (e.g., cavitation bubbles, laser-generated bubbles)

Interfacial layer: medium of arbitrary thickness coating a bubble

Bubbles are present inside a variety of soft materials and biological media. From the bubbles created upon decompression of magma in a volcanic eruption (Ichihara 2008) to those generated in the synovial fluid when we crack our joints (Kawchuk et al. 2015), these fascinating objects challenge scientists to understand and control their behavior.

The ability to control bubble dynamics underpins a number of industrial processes in which bubbles grow or undergo collapse within complex fluids. For instance, the expansion of gas bubbles in a polymeric liquid is central to the production of polymer foams (Everitt et al. 2003), and the dispersion of carbon nanotubes by ultrasonication is affected by cavitation and vapor bubble collapse, which cause nanotube scission (Pagani et al. 2012). Microscopic bubbles injected in the human body can be manipulated with ultrasound to deliver drugs at otherwise inaccessible locations, for instance, across the blood–brain barrier (Choi et al. 2011). In this case, and for many other medical applications of ultrasound (Coussios & Roy 2008), a deep understanding of bubble dynamics near or within soft tissue is vital to the outcome of a procedure. Cavitation is also involved in biological processes that we have only recently begun to understand. The cell membrane can absorb mechanical energy from an ultrasound wave, leading to bubble formation in the intramembrane space between the two lipid leaflets that make up the membrane (Krasovitski et al. 2011). On a larger length scale, cavitation bubbles can occur in trees and plants under strong hydric evaporative stress and can cause an embolism in the water circulation (Tyree & Sperry 1989).

Soft and biological materials, including cells, tissues, colloidal suspensions, polymer solutions, and gels, exhibit a behavior intermediate between that of a fluid and that of a solid, and are therefore characterized by an elasticity as well as a viscosity. The mechanical properties of such viscoelastic materials typically also depend on the amplitude and the rate of the applied deformation. Rheology is the study of the complex response to flow and deformation of these materials, and of the microscopic origin of this response (Chen et al. 2010). The rheological behavior of a viscoelastic material can be nonlinear and cause dramatic changes in bubble dynamics, which is in itself highly nonlinear even in simple fluids (Plesset & Prosperetti 1977). In addition, the interaction of bubbles with soft and biological matter occurs in a variety of geometries and configurations (**Figure 1**), as in some of the examples mentioned above. Bubbles can be embedded in a viscoelastic medium, can be coated by a viscoelastic interfacial layer, or can be in the proximity of a soft viscoelastic boundary.

The review covers recent developments on the effect of the medium rheology and of soft confinement on bubble dynamics, focusing in particular on the resonant behavior of bubbles as an exquisitely sensitive probe of their surroundings.

2. BUBBLE DYNAMICS IN A VISCOELASTIC MEDIUM

Here we introduce the governing equation of spherical bubble dynamics in an incompressible medium. For a Newtonian fluid, the governing equation reduces to the famous Rayleigh–Plesset equation (Plesset & Prosperetti 1977), a remarkable example of a solution of the Navier–Stokes equation in spherical coordinates. In this formulation, it is easy to specify the material properties of the surrounding medium and of an interfacial layer through the stress tensor, $\boldsymbol{\tau}$, and the interfacial stress tensor, $\boldsymbol{\tau}_s$, respectively (Section 2.1). We discuss some examples of linear and nonlinear constitutive models for $\boldsymbol{\tau}$ and highlight the effects of viscoelastic properties of the medium on bubble dynamics (Section 2.2). The role of the interfacial stress $\boldsymbol{\tau}_s$ is discussed in Section 3.2. Measurements of bubble dynamics in viscoelastic media are presented, with a particular focus on experiments in which the rheological properties of the medium are obtained from the bubble response (Section 2.3).

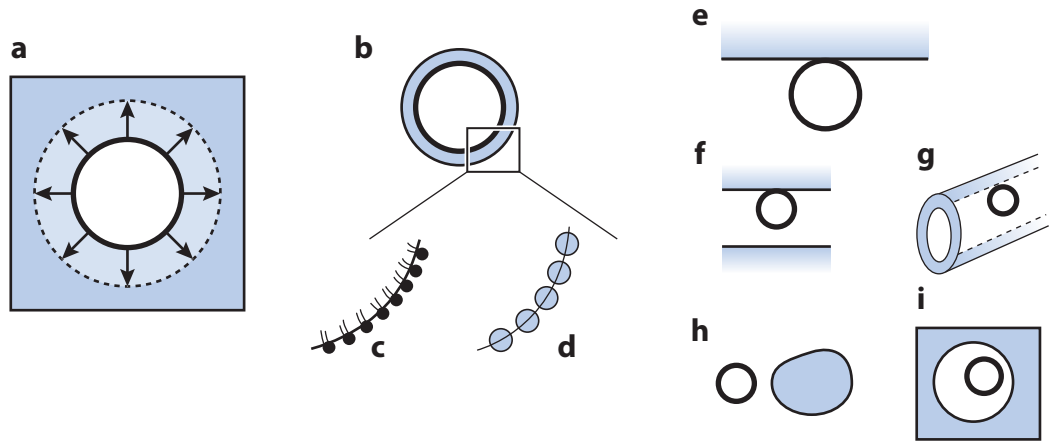

Figure 1

Bubble dynamics in soft confinement. (*a*) A bubble embedded in a viscoelastic medium (*blue*) in which the bubble radius can evolve. (*b*) A bubble coated with a viscoelastic interfacial layer. Examples include (*c*) lipid monolayers and (*d*) particle monolayers. Panels *e–i* show different geometrical examples of confinements: (*e*) a bubble near a viscoelastic boundary, (*f*) a bubble between parallel plates, (*g*) a bubble in a compliant tube, (*h*) a bubble near a suspended, deformable object, and (*i*) a bubble in a cavity within a viscoelastic material.

2.1. Governing Equation of Bubble Dynamics in a Viscoelastic Medium

We consider a spherical bubble in an incompressible, homogeneous, viscoelastic medium. We define a spherical coordinate system whose origin is at the center of the bubble, with r, θ, and ϕ being the radial, azimuthal, and polar coordinates, respectively. The position of the bubble is fixed and only its radius, R, changes in time, generating a purely radial velocity field, $\mathbf{u} = (u, 0, 0)$. From the continuity equation, $\frac{1}{r^2}\frac{\partial}{\partial r}(r^2 u) = 0$, with the boundary condition $u(r = R) = \dot{R}$, where the dot denotes derivative with respect to time, it follows that the velocity is $u(r, t) = R^2\dot{R}/r^2$. Substituting $u(r, t)$ into the radial component of the momentum equation,

$$\rho\left(\frac{\partial u}{\partial t} + u\frac{\partial u}{\partial r}\right) = -\frac{\partial p}{\partial r} + (\nabla\cdot\boldsymbol{\tau})_r\,, \qquad 1.$$

where $(\nabla\cdot\boldsymbol{\tau})_r$ is the radial component of $\nabla\cdot\boldsymbol{\tau}$, the divergence of the deviatoric stress tensor, given by $(\nabla\cdot\boldsymbol{\tau})_r = \frac{1}{r^2}\frac{\partial}{\partial r}(r^2\tau_{rr}) - \frac{\tau_{\theta\theta}+\tau_{\phi\phi}}{r}$, and integrating with respect to r gives

$$\rho\left(R\ddot{R} + \frac{3}{2}\dot{R}^2\right) = p(R) - p_\infty + \int_R^\infty (\nabla\cdot\boldsymbol{\tau})_r\, \mathrm{d}r, \qquad 2.$$

which is valid for any rheology of the surrounding medium. Here p_∞ is the pressure in the medium far from the bubble, and $p(R)$ is the pressure in the medium at the bubble interface, obtained from the balance of normal stress at the interface,

$$p(R) - (\nabla_\mathrm{s}\cdot\boldsymbol{\tau}_\mathrm{s})_r - \tau_{rr}(R) = p_\mathrm{g}, \qquad 3.$$

where p_g is the gas pressure in the bubble; viscous effects in the gas have been neglected. In this equation, the contribution of the interface appears through the radial component of the surface divergence of the interfacial stress (Edwards et al. 1991), given by $(\nabla_\mathrm{s}\cdot\boldsymbol{\tau}_\mathrm{s})_r = -(\tau_{\mathrm{s},\theta\theta} + \tau_{\mathrm{s},\phi\phi})/R$. We discuss the constitutive laws for the interfacial stress in Section 3.2 in the case of bubbles coated with a viscoelastic interfacial layer. For uncoated bubbles, the interfacial stress reduces to the surface tension of the gas–liquid interface, γ: $\boldsymbol{\tau}_\mathrm{s} = \gamma\mathbf{I}_\mathrm{s}$, where $\mathbf{I}_\mathrm{s}$ is the surface unit tensor; for

a spherical bubble, we have $\mathbf{I}_s = \mathbf{e}_\theta\mathbf{e}_\theta + \mathbf{e}_\phi\mathbf{e}_\phi$. Equation 3 then reduces to

$$p(R) + \frac{2\gamma}{R} - \tau_{rr}(R) = p_g. \qquad 4.$$

Inserting this equation in Equation 2, one gets

$$\rho\left(R\ddot{R} + \frac{3}{2}\dot{R}^2\right) = p_g - p_\infty - \frac{2\gamma}{R} + \tau_{rr}(R) + \int_R^\infty (\nabla\cdot\boldsymbol{\tau})_r \, \mathrm{d}r. \qquad 5.$$

In the linear regime of deformation of a viscoelastic medium, $\boldsymbol{\tau}$ is traceless, $\tau_{\theta\theta} + \tau_{\phi\phi} = -\tau_{rr}$; hence we have $(\nabla\cdot\boldsymbol{\tau})_r = \frac{\partial\tau_{rr}}{\partial r} + \frac{3\tau_{rr}}{r}$. With these assumptions, Equation 2 simplifies to (Prosperetti 1982)

$$\rho\left(R\ddot{R} + \frac{3}{2}\dot{R}^2\right) = p_g - p_\infty - \frac{2\gamma}{R} + 3\int_R^\infty \frac{\tau_{rr}}{r}\,\mathrm{d}r. \qquad 6.$$

This equation governs the dynamics of a spherical bubble in an incompressible medium with arbitrary rheological properties, provided that the stress tensor is traceless. Following, e.g., Keller & Miksis (1980), one can obtain a more general governing equation that also accounts for compressibility effects of the medium surrounding the bubble.

The gas pressure is a function of the bubble radius, and it depends on the thermal properties of the gas at the frequency of the acoustic driving. In this review, thermal dissipation effects due to the gas are effectively accounted for through a polytropic exponent κ, such that we have $p_g = p_{g,0}(R_0/R)^{3\kappa}$, $p_{g,0} = p_0 + 2\gamma/R_0$ being the gas pressure at equilibrium. The polytropic exponent is equal to 1 for isothermal compression of the gas and equal to the ratio of the heat capacities at constant pressure and at constant volume for adiabatic compression. We refer the reader to Prosperetti (1977) for the full theoretical treatment of thermal effects.

The rheological behavior of the medium is specified by introducing the constitutive equation that relates the stress, $\boldsymbol{\tau}$, to the strain, $\boldsymbol{\varepsilon}$, and the strain rate, $\dot{\boldsymbol{\varepsilon}}$. Because we have assumed a flow field with spherical symmetry, the only nonzero component of the strain rate is $\dot{\varepsilon}_{rr} = \partial u/\partial r = -2R^2\dot{R}/r^3$. Note that the mode of deformation of the medium around a spherical bubble is pure extension (biaxial extension upon expansion, uniaxial extension upon compression). Integration with respect to time gives the corresponding component of the strain, $\varepsilon_{rr}(r) = \int_0^t (\partial u/\partial r)\,\mathrm{d}t' = -2(R^3 - R_0^3)/3r^3$.

2.2. Effect of the Medium Rheology on Bubble Response

Bubbles are extremely sensitive probes of their surroundings, and the changes in bubble dynamics due to the rheological properties of the medium can indeed be dramatic. To illustrate this, we first recall the case of a Newtonian fluid, to introduce the analogy between an acoustically driven bubble and a harmonic oscillator (Section 2.2.1). Although this analogy is limited to the case of small-amplitude oscillations, it is a simple yet powerful tool to reveal the effects of the surroundings on bubble response. We then review some linear and nonlinear constitutive models (Sections 2.2.2 and 2.2.3), focusing primarily on harmonic driving of bubbles and their resonant behavior as a probe of the effect of medium rheology.

2.2.1. Small-amplitude oscillations in a Newtonian fluid. For an incompressible, Newtonian liquid of shear viscosity η, the radial component of the stress tensor is $\tau_{rr} = 2\eta\dot{\varepsilon}_{rr}$. Substituting this constitutive equation in Equation 6, the familiar Rayleigh–Plesset equation is obtained (Plesset &

Prosperetti 1977):

$$\rho\left(R\ddot{R}+\frac{3}{2}\dot{R}^2\right)=p_g-p_\infty-\frac{2\gamma}{R}-\frac{4\eta\dot{R}}{R}. \quad 7.$$

Creep: time-dependent increase in strain for a step increase in stress

For the case of harmonic driving of bubbles in acoustic fields, the pressure far from the bubble is $p_\infty = p_0 + p_a(t)$, where p_0 is the ambient pressure, and the acoustic pressure $p_a(t) = \Delta p \sin(\omega t)$ has amplitude Δp and angular frequency $\omega = 2\pi f$, where f is the frequency. The Reynolds number based on the equilibrium bubble radius, R_0, is $Re = \rho R_0^2\omega/\eta$. A bubble undergoing volumetric oscillations as a result of harmonic driving can be simply thought of as a forced harmonic oscillator, where the mass corresponds to the inertia of the fluid displaced by the bubble, and the spring corresponds to the restoring force due to the compression of the gas inside the bubble and surface tension (Leighton 1994). For sufficiently small amplitude of the acoustic forcing, $\Delta p/p_0 \ll 1$, the oscillatory response of the bubble can be assumed to be linear. The temporal evolution of the radius $R(t) = R_0 + \Delta R(t)$ can then be written as $R(t) = R_0[1 + x(t)]$ with $x(t) = x_0 \sin(\omega t + \varphi)$, where φ is the phase shift between the acoustic forcing and the radial oscillations, and the amplitude of oscillations is small, $x_0 = \Delta R/R_0 \ll 1$. Perturbation analysis to first order in the small parameter x returns the equation for the amplitude $x(t)$ in the form of a damped harmonic oscillator, $\ddot{x} + 2\beta\dot{x} + \omega_0^2 x = -\Delta p \sin(\omega t)/\rho R_0^2$, where β is the damping coefficient and ω_0 is the natural frequency (Prosperetti 1977). The natural frequency is given by

$$\omega_0^2=\frac{1}{\rho R_0^2}\left[3\kappa p_0+\frac{2(3\kappa-1)\gamma}{R_0}\right]. \quad 8.$$

If surface tension effects are negligible, the Minnaert frequency ω_M, given by $\omega_M^2 = 3\kappa p_0/\rho R_0^2$, is recovered. If the only damping mechanism is viscous dissipation, the damping coefficient is simply given by $\beta = \beta_{vis} = 2\eta/\rho R_0^2$. Damping in a Newtonian liquid may also include acoustic and thermal contributions, as described by Prosperetti (1977). The equation for the resonance curve of the bubble, which is the amplitude of bubble oscillations as a function of the applied frequency, is given by

$$x_0(\omega)=\frac{\Delta p}{\rho R_0^2}\frac{1}{\sqrt{\left(\omega_0^2-\omega^2\right)^2+4\beta^2\omega^2}}. \quad 9.$$

The frequency for which the amplitude of oscillations is a maximum, i.e., the resonance frequency, differs from the natural frequency because of damping and is obtained from Equation 9 as $\omega_{res}^2 = \omega_0^2 - 2\beta^2$.

2.2.2. Linear viscoelastic models. A simple linear constitutive model that includes viscous and elastic effects and captures creep behavior is the Kelvin–Voigt model (Macosko 1994). The radial component of the stress tensor is given by $\tau_{rr} = 2(G\varepsilon_{rr} + \eta\dot{\varepsilon}_{rr})$, where G is the shear modulus of the medium. The behavior described by this model is that of a spring and a dashpot in parallel, where the spring causes the material to recover its original configuration after deformation. It is therefore a model for predominantly solid materials and is suitable for soft tissue, which generally recovers its original configuration after the stress is removed.

The Kelvin–Voigt model can be simply combined with the momentum balance, Equation 6, to give a governing equation for a bubble in an incompressible, linear viscoelastic medium:

$$\rho\left(R\ddot{R}+\frac{3}{2}\dot{R}^2\right)=p_g-p_\infty-\frac{2\gamma}{R}-\frac{4\eta\dot{R}}{R}+\frac{4}{3}G\frac{R^3-R_0^3}{R^3}. \quad 10.$$

The assumption of a linear relationship between stress and strain and the use of Equation 6, both valid for small deformations, imply that also Equation 10 is only valid for small-amplitude

oscillations, $\Delta R/R_0 \ll 1$. Linearization of Equation 10, following the same perturbation analysis outlined in Section 2.2.1, gives the natural frequency:

Relaxation: time-dependent decrease in stress for a step increase in strain on a characteristic timescale, $\lambda = \eta/E$

$$\omega_0^2 = \frac{1}{\rho R_0^2}\left[3\kappa p_0 + \frac{2(3\kappa - 1)\gamma}{R_0} + 4G\right], \qquad 11.$$

which reduces to Equation 8 for $G = 0$. For a given bubble radius, the natural frequency increases with increasing G, as a result of the increased stiffness of the system due to the solid-like elasticity of the surrounding medium (**Figure 2*a***). Yang & Church (2005) combined the Kelvin–Voigt constitutive model with the Keller–Miksis equation to also account for compressibility effects and performed perturbation analysis to obtain the resonance frequency and damping coefficients for this case.

Another simple, linear viscoelastic model is the linear Maxwell model (Macosko 1994), represented by a spring and a dashpot in series, suitable for predominantly liquid materials. The constitutive equation is given by $\lambda\dot{\tau}_{rr} + \tau_{rr} = 2\eta\dot{\varepsilon}_{rr}$, where λ is the relaxation time of the material, given by $\lambda = \eta/G$. The dimensionless number comparing the relaxation timescale of the material with the characteristic timescale of the flow is the Deborah number, which for harmonic driving at frequency ω is $De = \lambda\omega$. The Deborah number measures the ability of the material to relax back to its initial state during one cycle of the acoustic forcing. Despite its simplicity, the Maxwell model combined with Equation 6 does not yield an ordinary differential equation for the bubble radius. Fogler & Goddard (1970) were the first to obtain and numerically solve the integro-differential equation for the radial dynamics, with the aim of investigating bubble collapse in polymer processing. Allen & Roy (2000a) reduced the problem to a set of coupled ordinary differential equations and used a multiple-scale perturbation method to obtain an equation for the resonance frequency of the bubble. The equation was solved numerically to obtain resonance curves for parameters of relevance to medical applications. For small-amplitude forcing ($Re = 0.1$) such that the response in a Newtonian fluid ($De = 0$) was linear, a softening nonlinearity was observed for the Maxwell fluid, with the nonlinear effect increasing with the elasticity of the medium ($De = 1 - 3$). This result highlights a strong effect of the medium rheology on bubble dynamics even for small-amplitude forcing.

To reflect the fact that many soft materials have intermediate behavior between that of a fluid and that of a solid, one can combine the Kelvin–Voigt and Maxwell models to obtain the standard linear solid model. In this model, a spring in parallel to a Maxwell element (spring and dashpot in series) confers solid-like behavior to the system. The constitutive equation, shown in **Table 1**, has been combined with the Keller–Miksis equation by Hua & Johnsen (2013). They found that when the term in $\dot{\tau}_{rr}$ is sufficiently large, nonlinear effects become important and the steady-state oscillation frequency after a Rayleigh collapse differs from the natural frequency, with a nontrivial dependence on Re and De.

2.2.3. Nonlinear viscoelastic models. Many applications of bubble dynamics in viscoelastic media involve relatively large deformations, for instance, cavitation in tissues for noninvasive therapy and drug delivery (Coussios & Roy 2008). To model these situations, one can combine the equation governing bubble dynamics with a nonlinear constitutive model, valid for large strains. In this case, Equation 5 with a general form of the stress tensor is used, as the assumption of a traceless stress tensor may not be valid. Equation 5 is often modified following Keller & Miksis (1980) to account for compressibility effects, which can also become important for large strains.

Several authors have considered a nonlinear version of the Maxwell model in the context of bubble dynamics (Allen & Roy 2000b, Jiménez-Fernández & Crespo 2005, Naude & Méndez 2008, Warnez & Johnsen 2015). In this model, referred to as the upper-convected Maxwell model,

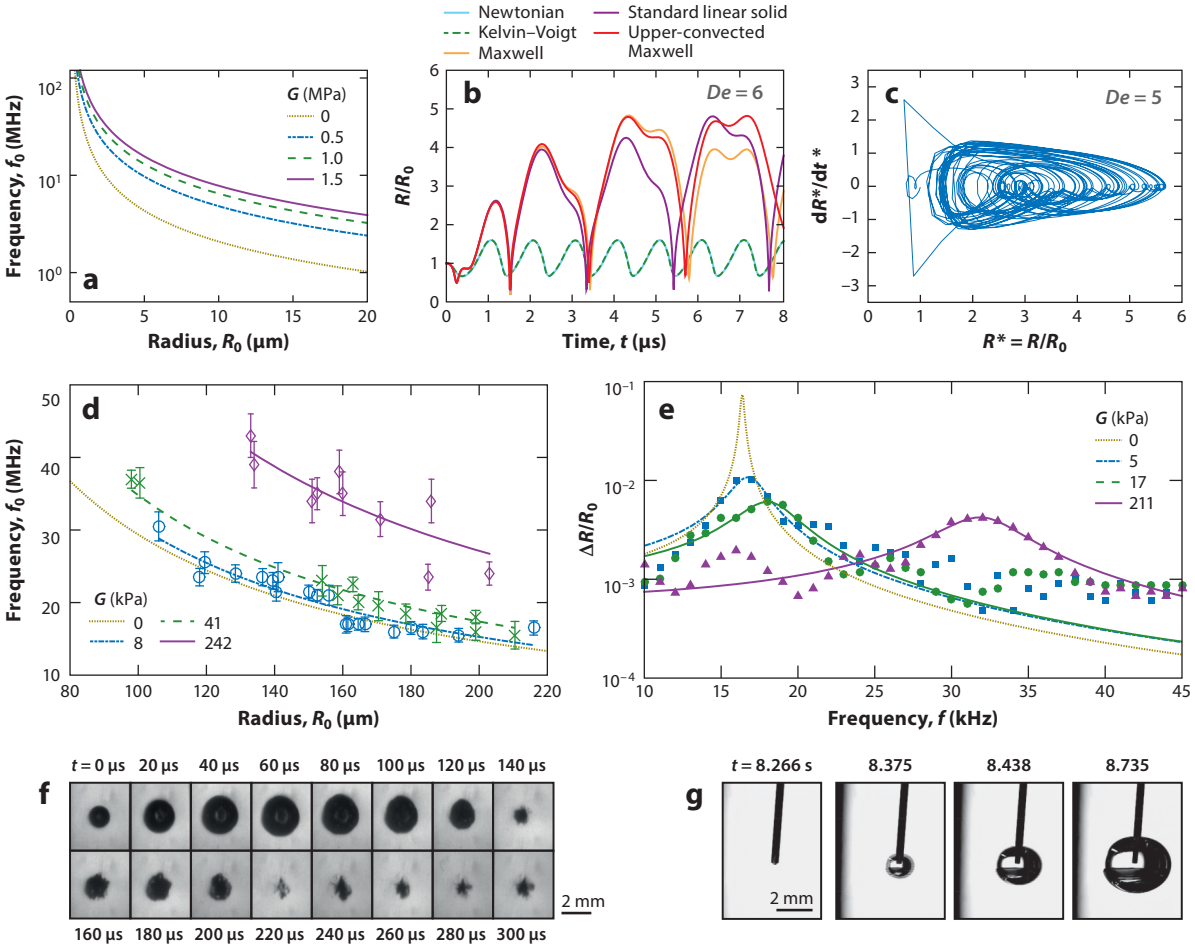

Figure 2

Bubble dynamics in a viscoelastic medium. (*a*) Prediction of the change in resonance frequency as a function of bubble radius for a Kelvin–Voigt, linear viscoelastic solid. Data plotted using Equation 11 and parameters taken from Yang & Church (2005). (*b*) Comparison of Newtonian, Kelvin–Voigt, Maxwell, standard linear solid, and upper-convected Maxwell models. (*c*) Chaotic behavior of a bubble undergoing large-amplitude oscillations in a viscoelastic fluid. (*d*) Experimental measurement of the change in resonance frequency as a function of bubble radius in agarose gels with increasing G. The experimental data are fitted (*lines*) to Equation 11 to extract G. (*e*) Experimental resonance curves from small-amplitude bubble oscillations in agarose gels with increasing G. The experimental data are fitted (*lines*) to Equation 9 to extract G and η. (*f*) Collapse of a laser-generated bubble in a polyacrylamide gel. (*g*) Cavitation rheology uses quasi-static bubble injection to measure the elastic modulus. Panels *b–g* adapted with permission from (*b*) Warnez & Johnsen (2015), copyright AIP Publishing; (*c*) Naude & Méndez (2008), copyright Elsevier; (*d*,*e*) Jamburidze et al. (2017), copyright Royal Society of Chemistry; (*f*) Brujan & Vogel (2006); and (*g*) Kundu & Crosby (2009), copyright Royal Society of Chemistry. Abbreviations: *De*, Deborah number; G, shear modulus; η, shear viscosity.

the time derivative of the stress tensor is replaced with the upper-convected time derivative to respect frame invariance (Macosko 1994). Using this model, Allen & Roy (2000b) showed that for harmonic forcing near resonance with $Re = 2.5$ and $De = 3$, the linear and nonlinear Maxwell models give the same prediction for small-amplitude forcing ($p_a = 50$ kPa); on the contrary, for larger forcing amplitudes ($p_a = 200$ kPa), the nonlinear model predicts stable oscillations while the linear model predicts explosive growth. Since such prediction is inconsistent with the underlying

Table 1 Linear constitutive models

Model	Constitutive equation	Properties
Newtonian	$\tau_{rr} = 2\eta\dot{\varepsilon}_{rr}$	Newtonian liquid
Kelvin–Voigt[a]	$\tau_{rr} = 2G\varepsilon_{rr} + 2\eta\dot{\varepsilon}_{rr}$	Viscoelastic solid; creep behavior
Maxwell[b]	$\lambda\dot{\tau}_{rr} + \tau_{rr} = 2\eta\dot{\varepsilon}_{rr}$	Viscoelastic liquid; stress relaxation
Standard linear solid[c]	$\lambda\dot{\tau}_{rr} + \tau_{rr} = 2G\varepsilon_{rr} + 2\eta\dot{\varepsilon}_{rr}$	Predicts both creep and stress relaxation

[a]Used by Yang & Church (2005), Hamaguchi & Ando (2015), and Jamburidze et al. (2017).
[b]Used by Fogler & Goddard (1970) and Allen & Roy (2000a).
[c]Used by Hua & Johnsen (2013).

assumption of small strain for the linear model, the comparison highlights the importance of choosing a suitable nonlinear model for large strains. **Figure 2*b*** shows a comparison of the evolution of the bubble radius during harmonic driving at $p_a = 400$ kPa for Newtonian ($De = 0$), Kelvin–Voigt, Maxwell, standard linear solid, and upper-convected Maxwell models ($De \approx 6$) (Warnez & Johnsen 2015). The models without relaxation (Newtonian and Kelvin–Voigt) show limited nonlinear behavior, while for the models that include relaxation, the effect on the amplitude and frequency of oscillations is dramatic. For sufficiently large Deborah numbers, the nonlinear Maxwell model predicts aperiodic oscillations and chaotic behavior (Jiménez-Fernández & Crespo 2005, Naude & Méndez 2008), as shown in **Figure 2*c*** ($De = 5$), because in this regime the forcing period, $\tau \sim \omega^{-1}$, is much shorter than the relaxation time of the material, λ, meaning that the stress continues to build up cycle after cycle of oscillation.

Nonlinear constitutive equations that describe more complex rheological responses have been combined with the equation governing bubble dynamics (Gaudron et al. 2015, Warnez & Johnsen 2015, Estrada et al. 2018) but are not discussed here.

2.3. Experimental Results

Motivated by applications in polymer processing, early experimental studies on bubble dynamics in viscoelastic liquids have focused primarily on bubble collapse. These studies have been reviewed elsewhere (Macosko 1994) and are not covered here. More recently, the influence of the mechanical properties of biological fluids and tissues on cavitation and bubble dynamics has gained widespread interest because of its relevance in many biomedical applications, for instance, tissue ablation by high-intensity focused ultrasound, ophthalmic microsurgery, and microbubble-enhanced ultrasound imaging; Brujan (2010) has reviewed comprehensively the topic of cavitation for biomedical and bioengineering applications. Here we focus on recent experiments that have used bubble dynamics as a probe of the rheological properties of a viscoelastic medium.

Because in general the mechanical response of soft materials depends on the rate of deformation, the rheological properties need to be measured at the frequency of interest. However, standard instruments typically cannot reach the high strain rates (10^3–10^6 s^{-1}) characteristic of bubble collapse and ultrasound-driven bubble dynamics. The theoretical predictions presented above suggest that experiments on oscillatory bubble dynamics in viscoelastic media can provide measurements of rheological properties at high frequency. While such a technique has not yet been benchmarked and adopted widely in applications, a few studies have shown the viability of this approach, termed "acoustic microrheology" (Strybulevych et al. 2009). Strybulevych et al. (2009) recorded the resonance curves of millimetric bubbles in agar gel by measuring the acoustic response of the bubble as a function of frequency. They fitted the resonance curve and the damping

coefficient given by the linear Kelvin–Voigt model to obtain the material properties. Hamaguchi & Ando (2015) recorded optically resonance curves using a constant ultrasound frequency while the bubble radius slowly increased over time due to gas transfer into the bubble. Values of shear modulus and shear viscosity were extracted by fitting Equation 9 to the data. Jamburidze et al. (2017) recorded resonance curves of bubbles excited by ultrasound at small pressure amplitudes ($p_a < 1$ kPa) in agarose gels to ensure that the deformation of the material remained in the linear regime. The resonance curves were fitted to Equation 9 to extract the viscoelastic properties (see **Figure 2*d***). The measurement was found to be robust by comparing the results from different bubbles, as shown in **Figure 2*e***.

Bubble collapse is also sensitive to the rheology of the surrounding medium, but the analysis of the experimental results to infer viscoelastic properties can be challenging. Controlled experiments with direct visualizations of bubble collapse in polyacryalmide gels (**Figure 2*f***) showed that the maximum radius of the laser-generated bubble decreased with increasing elastic modulus, and the oscillation period of the bubble was reduced (Brujan & Vogel 2006), qualitatively in agreement with Equation 11.

Recently, a method for high–strain rate rheometry based on inertial cavitation has been demonstrated, in which time-resolved data for the temporal evolution of the radius are fitted to the prediction of the equation governing bubble dynamics, combined with a suitable nonlinear constitutive model (Estrada et al. 2018).

Finally, another technique that uses bubbles to probe mechanical properties of soft materials, called "cavitation rheology" (Zimberlin et al. 2007), uses quasi-static bubble injection to determine the elastic modulus of a soft material by monitoring the pressure in the bubble at the onset of a mechanical instability (see **Figure 2*g***). This elegant technique does not provide information on the frequency dependence of the mechanical properties.

One of the advantages of using bubbles as rheological probes is that they can provide information on the local properties of inhomogeneous materials. This is advantageous for soft and biological materials, which often have complex microstructures. The knowledge of the effect of high-rate deformation on the microstructure of an inhomogeneous material is still limited. Future research should fill this gap, as well as the link between microscale phenomena and rheological response.

3. BUBBLE DYNAMICS WITH A VISCOELASTIC INTERFACE

Stable bubble dispersions are central in the formulated products industry and in biomedical imaging. Small bubbles are stabilized against dissolution by coating their interface with a layer of surface-active material. In Section 2, we have seen that for the case of bubble dynamics in a viscoelastic medium, theoretical work has predated some of the experimental developments. In contrast, the effect of an interfacial coating on bubble dynamics has been first observed experimentally, motivating subsequent efforts to develop predictive models. To reflect this, we report the experimental observations in this section before the theoretical models. Surface viscoelasticity significantly increases the resonance frequency and damping, and the coating exacerbates nonlinear oscillation effects (Section 3.1), which is challenging for modeling (Section 3.2). This section also covers the recently emerging area of particle-stabilized bubbles (Section 3.3).

3.1. Experimental Coating Effects

Coated bubbles are generally micrometric to millimetric in radius and thus resonate at several kilohertz to several megahertz. It is therefore difficult to optically resolve their oscillations. Alternative methods to characterize their resonance properties rely either on purely acoustical measurements

or on light scattering (Tu et al. 2009). With the advent of high-speed cameras, direct imaging has become possible using either streak cameras, recording one single line of pixels through a bubble up to 100 MHz, or ultra-high-speed cameras, recording images up to 25 MHz, which becomes sufficient to resolve several cycles of oscillations (Versluis 2013).

Monolayer: single layer of molecules or particles adsorbed at an interface or surface

Shell: curved layer of thickness much larger than the molecular size, such that it can be treated as a continuum across its thickness

3.1.1. Changes in linear response. Compared to uncoated bubbles, coated bubbles display a larger resonance frequency, a lower amplitude of response, and a larger damping. Many studies have characterized coated microbubbles used as ultrasound contrast agents for medical imaging. These agents have different kinds of coating: a protein layer (**Figure 3*a***), a polymer shell (**Figure 3*b***), or a thin lipid monolayer. As discussed in Section 3.2, there are two kinds of models to describe the effect of the coating on bubble oscillations: models considering shells as three-dimensional (3D) media of finite thickness, adapted to polymer or protein coatings, and models considering an infinitely thin interface, with 2D properties, adapted to lipid monolayers. However, a common point of all models is to ascribe to coatings two contributions, an elastic and a viscous one, and the experimental studies have all fitted their measurements to estimate both of these contributions.

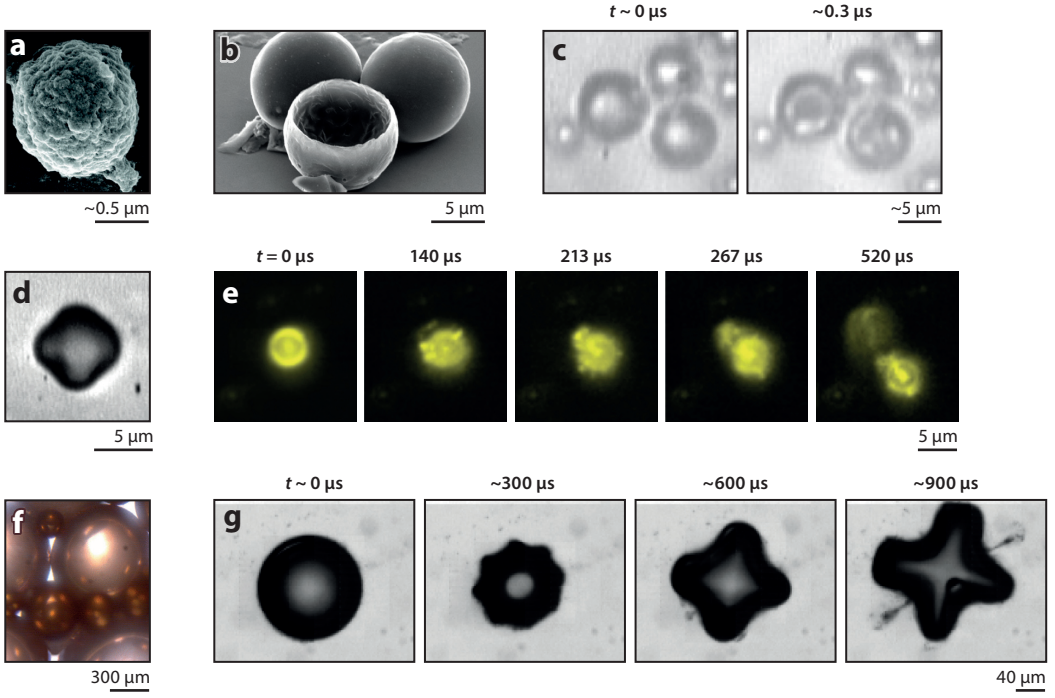

Figure 3

Examples of coated bubbles. (*a*) Electron micrograph of a microbubble coated with a protein layer. (*b*) Polymer capsules, which are shells of polymer-coated bubbles. (*c*) Snapshots of coated microbubbles under ultrasound at two moments during an acoustic cycle: in the inflated state (*left*) and in the buckled state with wrinkles (*right*). (*d*) Nonspherical surface modes displayed by a lipid-coated bubble under ultrasound. (*e*) Lipid shedding from a microbubble under ultrasound. (*f*) Bubbles coated by magnetic nanoparticles. (*g*) Directional particle shedding from the antinodes of a particle-coated bubble undergoing shape oscillations. Panels adapted with permission from (*a*) Cavalieri et al. (2008), copyright American Chemical Society; (*b*) Böhmer et al. (2006), copyright Elsevier; (*c*) Marmottant et al. (2011), copyright Acoustical Society of America; (*d*) Dollet et al. (2008), copyright Elsevier; (*e*) Luan et al. (2014), copyright Elsevier; (*f*) Zhao et al. (2009), copyright American Physical Society; and (*g*) Poulichet & Garbin (2015).

In the context of ultrasound contrast agents, de Jong et al. (1992) performed one of the first acoustic characterizations of a suspension of bubbles coated by a protein layer, and they provided an estimate of an elastic contribution of such layers. Frinking & de Jong (1998) also characterized bubbles coated with a protein layer (**Figure 3*a***) and extended the analysis by de Jong et al. (1992) by including a dissipative contribution from the coating. Hoff et al. (2000) studied polymer-coated bubbles, both experimentally and theoretically. They fitted their measurements by Church's (1995) model (Section 3.2) in the limit of a thin shell to obtain a shell shear modulus and a shell viscosity. For bubbles coated with a lipid monolayer, Gorce et al. (2000) fitted a shell stiffness and friction parameter.

All these studies characterized a polydisperse population of coated bubbles by purely acoustic means. The drawback of such methods is that the influence of the coating on the acoustic properties of the bubbles is convoluted by the bubble size distribution. Parrales et al. (2014) used microfluidic flow–focusing techniques to produce fairly monodisperse lipid-coated bubble suspensions of relevant diameter for medical application (with a mean diameter of 6 μm). Measuring the attenuation coefficient, they had a good estimate of the elasticity and viscosity of lipid monolayers.

To go beyond purely acoustical measurements, Morgan et al. (2000) insonified bubbles coated with a lipid monolayer and simultaneously imaged their oscillations along their centerlines using a streak camera. They compared these measurements with a viscoelastic shell model, using shell elastic and viscous moduli as two fitting parameters. They found that shell viscosity increased with bubble radius. Van der Meer et al. (2007) insonified bubbles coated with a lipid monolayer at amplitude below 40 kPa to minimize nonlinear effects, imaged their oscillation with an ultra-high-speed camera, measured the oscillation amplitude as a function of frequency for individual bubbles of different radii, obtained from them resonance frequencies and damping coefficients as a function of bubble radius, and fitted these data with a viscoelastic monolayer model. They found a surface elasticity of $\chi = 0.5 \pm 0.1$ N/m (see Section 3.2) and confirmed the increase of surface viscosity with increasing bubble radius.

In recent studies, bubbles of controlled coating composition have been synthesized, especially with lipids, and the influence of this composition has been quantified. For instance, van Rooij et al. (2015) used a method similar to that used by van der Meer et al. (2007) to characterize bubbles coated by two different lipids: 1,2-distearoyl-*sn*-glycero-3-phosphocholine (DSPC) and 1,2-dipalmitoyl-*sn*-glycero-3-phosphocholine (DPPC). These authors found that DSPC has a larger surface elasticity than DPPC. Lum et al. (2016) developed a different technique, using plasmonic bubbles, to investigate the surface rheology of lipid (the D•PC family) monolayers in the megahertz range: The decaying free oscillations of lipid-coated bubbles were measured by optical scattering methods, and the natural frequency and damping were fitted to measure surface elasticity and viscosity. They found an increase of elasticity with increasing carbon chain length, which they ascribed to the modification of intermolecular forces. **Figure 4*a*** illustrates their results and exemplifies that coating elasticity leads to a significant increase of the resonance frequency compared to the Minnaert frequency.

3.1.2. Nonlinear effects. In the context of medical imaging, nonlinear oscillations of coated bubbles have been studied to improve signal-to-noise ratio, because bubbles have a much more nonlinear response than the surrounding tissue. Second harmonic generation (emission at twice the forcing frequency) is the most classical nonlinearity. However, it is more attenuated, and less specific, than subharmonic emission (Shankar et al. 1998), which has thus received much attention.

Among the first researchers to identify such nonlinearities, Lotsberg et al. (1996) found evidence for a clear subharmonic signal for protein-coated bubbles, at lower pressure amplitude than the subharmonic threshold suggested by the theory for uncoated bubbles (Prosperetti 1974). Shankar

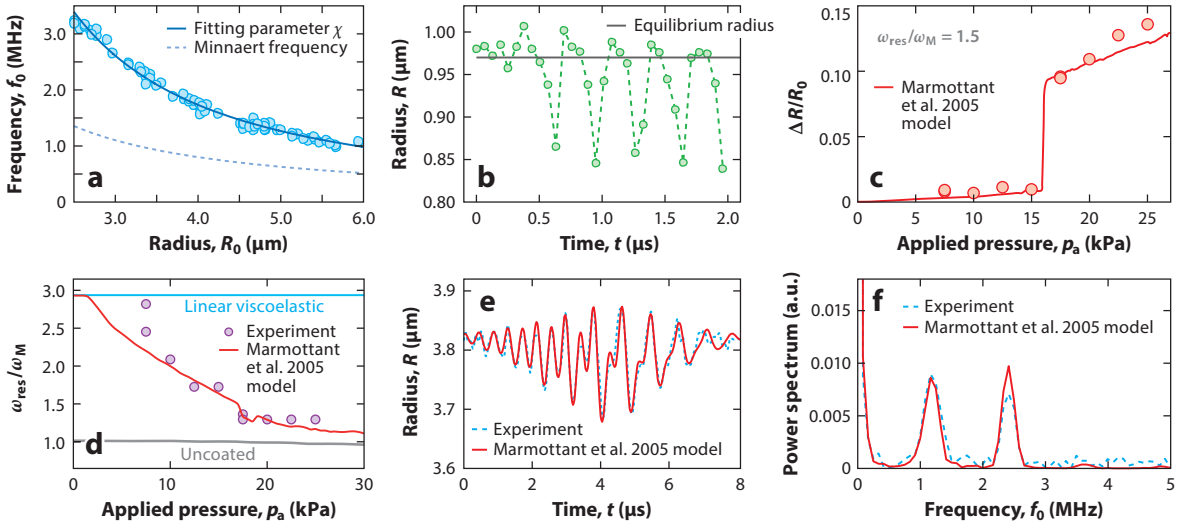

Figure 4

Linear and nonlinear responses of lipid-coated bubbles to an ultrasonic field. (*a*) Natural frequency of bubbles coated with 1,2-dipalmitoyl-*sn*-glycero-3-phosphocholine (DPPC) monolayers as a function of their radius. Data are replotted with permission from Lum et al. (2016), copyright American Chemical Society, and are fitted by Equation 12 with χ as fitting parameter (*dark-blue solid line*). (*b*) Compression-only behavior. The oscillation amplitude in the compression phase is much larger than in the expansion phase. Data replotted with permission from Marmottant et al. (2005), copyright Acoustical Society of America. (*c*) Relative oscillation amplitude as a function of applied pressure. The abrupt jump in amplitude represents the thresholding behavior. (*d*) Nonlinear resonance. The resonance frequency (here rescaled by the Minnaert frequency) decreases strongly at increasing applied pressure; the light-blue line corresponds to a model with linear surface viscoelasticity. (*e*,*f*) Subharmonic oscillations: (*e*) an illustration on a radius–time curve for $f = 2.4$ MHz and $p_a = 40$ kPa and (*f*) the corresponding power spectrum. In panels *c*–*f*, the red solid lines represent fits by Equation 7 with the effective surface tension given by Equation 13. Panels *c*–*f* adapted with permission from (*c*,*d*) Overvelde et al. (2010), copyright Elsevier, and (*e*,*f*) Sijl et al. (2010), copyright Acoustical Society of America.

et al. (1999) confirmed this fact and reported subharmonic backscattering at forcing amplitudes as low as 20 kPa. Beyond acoustical characterization, Sun et al. (2005) observed that lipid-coated bubbles undergo subharmonic oscillations using streak imaging; these were also reported by Sijl et al. (2010) from direct optical measurements (**Figure 4*e***).

While purely acoustical methods were efficient in revealing subharmonic emission from coated bubbles, ultra-high-speed imaging of oscillating coated bubbles revealed a wealth of other nonlinear effects, apparent already at very low forcing compared to uncoated bubbles, like subharmonics: compression-only, thresholding, and nonspherical oscillations, often associated with buckling or crumpling of the coating. Marmottant et al. (2005) revealed that bubbles coated with a lipid monolayer oscillate in a so-called compression-only manner, i.e., they compress more than they expand, compared to their equilibrium radius (**Figure 4*b***), in marked contrast with uncoated bubbles oscillating in a nonlinear fashion, which expand more than they compress. Emmer et al. (2007) showed that the relation between the oscillation amplitude of lipid-coated bubbles and the forcing amplitude is highly nonlinear: At forcing frequencies below their resonance frequency, lipid-coated bubbles hardly oscillate below a forcing threshold, above which the oscillation amplitude increases abruptly (**Figure 4*c***). Initially ascribed to size-dependent shell properties, this so-called thresholding nonlinear behavior, together with compression-only behavior, was later rationalized by Overvelde et al. (2010) in the general framework of nonlinear oscillations. This paper also showed that the resonance frequency of coated bubbles is a strongly decreasing function of the amplitude (both forcing and oscillation), reminiscent of a softening nonlinearity (**Figure 4*d***).

Above a certain forcing amplitude, bubbles display nonspherical oscillations. Like volumetric ones, these are significantly affected by surface viscoelasticity. For millimetric bubbles, Asaki et al. (1995) and Asaki & Marston (1997) showed that the presence of soluble and insoluble surfactants slightly changes the natural frequency, and increases the damping up to eight times, of a quadrupolar nonspherical mode. Dollet et al. (2008) showed that the nonspherical oscillations of lipid-coated microbubbles (**Figure 3*d***) display a subharmonic character, reminiscent of a parametric instability, but without shape mode selectivity, unlike uncoated bubbles (Versluis et al. 2010). Nonspherical shapes can also appear through buckling of the interfacial layer; indeed, Borden & Longo (2002) showed that lipid-coated bubbles buckle under slow deflation. Later, Marmottant et al. (2011) studied the buckling threshold of coated bubbles under ultrasound (**Figure 3*c***) and related this threshold to the buckling of spherical shells in solid mechanics. Moreover, under strong oscillation, the coating itself may rupture (Postema et al. 2004) or shed some material (Luan et al. 2014) (**Figure 3*e***).

3.2. Coating Models

Experimental developments on coated bubbles have motivated active modeling of the influence of the coating mechanical properties on bubble oscillations. There are excellent reviews on such models (e.g., Doinikov & Bouakaz 2011, Faez et al. 2013), and we refer the reader to them for full details on the many different models. In this section, our purpose is to outline the main physical motivations of the different generations of models.

As soon as it appeared that the resonance frequency and damping of coated bubbles were larger than those of uncoated ones, models ascribed elastic and viscous properties to the coating. This was done on a semiempirical basis by de Jong et al. (1992), and more rigorously by Church (1995), who considered a shell of finite thickness coating the bubble, considered as a viscoelastic solid and modeled by the linear Kelvin–Voigt constitutive law. Several variants issued from this model; readers are referred to, e.g., Hoff et al. (2000) or Morgan et al. (2000). These models generally lead to good fitting of the acoustic response of a polydisperse population of bubbles with thick shells.

A different assumption is to directly consider the coating as a 2D surface of negligible thickness, in the spirit of surfactant monolayer modeling (Langevin 2014), hence adapted to lipid-coated bubbles. Chatterjee & Sarkar (2003) modeled the interface as a Newtonian interface, $\boldsymbol{\tau}_s = \gamma \mathbf{I}_s + (\kappa_s - \mu_s)(\mathbf{I}_s : \mathbf{D}_s)\mathbf{I}_s + 2\mu_s \mathbf{D}_s$, where κ_s, μ_s, and $\mathbf{D}_s$ are the dilatational surface viscosity, the shear surface viscosity, and the surface deformation rate tensor, respectively. With this law, the radial component of the surface divergence of the interfacial stress becomes $(\mathrm{div}_s \boldsymbol{\tau}_s)_r = \frac{2\gamma}{R} + \frac{4\kappa_s \dot{R}}{R^2}$. Sarkar et al. (2005) then extended this model by including a surface dilatational elasticity through a compression modulus χ defined as $\chi = \mathrm{d}\gamma/\mathrm{d}\ln A$, where A is the bubble area. This amounts to changing surface tension, hitherto considered as constant, to an effective, radius-dependent surface tension, $\gamma(R) = \gamma(R_0) + \chi\left(\frac{R^2}{R_0^2} - 1\right)$, in Equation 4. Including this effective surface tension in Equation 7 yields a modified Rayleigh–Plesset equation for coated bubble oscillations. In particular, surface elasticity contributes to the resonance frequency as follows (compare with Equation 8):

$$\omega_0^2 = \frac{1}{\rho R_0^2}\left[3\kappa p_0 + \frac{2(3\kappa - 1)\gamma(R_0)}{R_0} + \frac{4\chi}{R_0}\right]. \qquad 12.$$

This equation served as a fitting formula to measure surface elasticity in several studies (van der Meer et al. 2007, van Rooij et al. 2015, Lum et al. 2016).

The optical observations of oscillating individual coated bubbles revealed a wealth of nonlinearities that the aforementioned models, with their linear description of surface viscoelasticity,

were unable to capture (**Figure 4*d***). Motivated by the discovery of the compression-only behavior (Section 3.1.2), a landmark study was performed by Marmottant et al. (2005). Inspired by the quasi-static behavior of insoluble monolayers of phospholipids in compression, they proposed the following phenomenological law for the effective surface tension:

$$\gamma(R) = \begin{cases} 0 & \text{for } R \le R_{\text{buckling}}, \\ \gamma(R_0) + \chi\left(\frac{R^2}{R_0^2} - 1\right) & \text{for } R_{\text{buckling}} \le R \le R_{\text{rupture}}, \\ \gamma_{\text{water}} & \text{for } R \ge R_{\text{rupture}}. \end{cases} \quad 13.$$

This accounts for (*a*) the appearance of buckling for a radius smaller than R_{buckling}, where the coating cannot sustain compression; (*b*) rupture of the coating for a radius larger than R_{rupture}, where the bubble behaves as if it were uncoated; and (*c*) an elastic regime in between. The resulting piecewise definition of the effective surface tension renders the model highly nonlinear. It was successful in predicting the nonlinearities of oscillating coated bubbles (**Figure 4**). This essentially comes from the fact that nonlinearities are enhanced by the abrupt change of properties at R_{buckling} and R_{rupture}. In the particular case of the subharmonic threshold, this reason for the good agreement between data and the model of Marmottant et al. (2005) was suggested by Sijl et al. (2010) and shown analytically by Prosperetti (2013). In the frame of this model, compression-only behavior is explained by the lower resistance in compression in the buckled state than in expansion, where elasticity has to be overcome; the strong decrease of resonance frequency with increasing amplitude was explained by the increasing influence of the softer buckled state as the oscillation amplitude increases (Overvelde et al. 2010).

More recent models aimed at capturing these nonlinearities with rigorous treatments of coating mechanics. Tsiglifis & Pelekasis (2008) modeled the coating as a nonlinear elastic solid and showed that a strain-softening constitutive law reproduces the decrease of resonance frequency with increasing amplitude. Other nonlinear models use radius-dependent surface elasticities (Stride 2008, Paul et al. 2010). Bending elasticity has also been included in recent models to understand the onset of nonspherical oscillations (Tsiglifis & Pelekasis 2011, Liu et al. 2012).

While all these models considered, essentially, coating as a viscoelastic solid, Doinikov & Dayton (2007) modeled it as a viscoelastic liquid using the Maxwell model. It is interesting to notice that their model was motivated by the fact that some experimental studies showed no significant difference of resonance frequency of coated bubbles compared to uncoated bubbles. However, at least two other physical effects can substantially change the resonance frequency, nonlinear effects (Section 3.1.2) and the vicinity of boundaries (Section 4.1), and these effects are difficult to disentangle from those of surface elasticity.

3.3. Acoustically Driven Particle-Stabilized Bubbles

Bubbles can also be stabilized against dissolution by solid particles instead of molecular surfactants, with the particles forming an armor on the interface, hence the name "armored bubbles" (Abkarian et al. 2007). The response of particle-stabilized bubbles to changes in pH, temperature, mechanical stress, and magnetic fields has been studied extensively, as reviewed by Fujii & Nakamura (2017), but it is only recently that the response to acoustic fields has been investigated.

Microbubbles stabilized by a monolayer of colloidal particles (nanoparticles or microparticles) have been found to exhibit an increased nonlinear response at low ultrasound pressure amplitudes (Stride et al. 2008, Poulichet & Garbin 2015). Because the particles prevent the bubble from contracting when they form a close-packed monolayer at the interface during compression, the oscillation amplitude is asymmetric around the equilibrium radius and is dominated by the

expansion of the bubble. This expansion-only behavior can be understood as the counterpart of the compression-only behavior observed for lipid-coated bubbles (see Section 3.1.2): While a surfactant monolayer offers minute resistance to compression beyond close packing because it easily buckles, monolayers of solid particles exert larger mechanical resistance to compression at small pressure amplitudes. For sufficiently large pressure amplitudes, particle-stabilized bubbles also undergo buckling (Poulichet & Garbin 2015) and can shed particles from their coating.

Microbubbles can be coated by a multilayer of particles, as is the case for the so-called magnetic bubbles (Zhao et al. 2009), which present a shell of magnetic nanoparticles a few tens of nanometers thick, shown in **Figure 3*f***. Magnetic bubbles can be manipulated with a magnetic field, oscillate in ultrasound, and shed nanoparticles, with potential applications to drug delivery (Gao et al. 2016).

The large-amplitude oscillations required for particle expulsion typically also cause shape oscillations of the bubbles. Particle-coated bubbles undergoing shape oscillations were found to exhibit directional particle expulsion from the antinodes of the shape oscillations (Gao et al. 2016, Poulichet et al. 2017), as shown in **Figure 3*g***.

The question of what constitutive models best describe the behavior of particle-coated bubbles remains open. An empirical model has been put forward to describe expansion-only behavior (Stride 2008), but models combining the governing equation for bubble dynamics with a constitutive model for a particle monolayer are not yet available. Progress is also limited because of a lack of experimental data suitable to test constitutive models.

4. BUBBLES NEAR VISCOELASTIC MATERIALS

Cavitation near hard boundaries is a classical topic in underwater acoustics and surface cleaning, reviewed by Blake & Gibson (1987). The interest in the interactions between bubbles and soft boundaries has recently been revived because of the growing number of biomedical and biological applications, ranging from ultrasound imaging and drug delivery to bubbles in plants and trees. This has driven studies on bubble dynamics in the soft-confinement conditions encountered in biomedical and biological systems. The proximity of a solid compliant boundary affects the dynamic response of bubbles in ultrasound (Section 4.1). Other examples of soft confinement include bubble dynamics inside compliant tubes such as blood vessels (Section 4.2), the interaction of bubbles with suspended cells or vesicles (Section 4.3), and bubble collapse in elastic cavities (Section 4.4).

4.1. Bubble Dynamics Near a Planar Viscoelastic Boundary

We begin with the case of a bubble near a planar boundary as the starting point for more complex geometries. As we will see, the effect of even the simplest confinement geometry is intricate. The effect of an infinitely rigid wall on the resonance of a single bubble is easy to model by the method of images (Strasberg 1953). The presence of the wall is equivalent to that of a fictitious second bubble that is the symmetric of the real bubble with respect to the wall. The velocity field in the liquid is then the superposition of the two fields created by each of the oscillating bubbles. Strasberg (1953) showed that the resonance frequency is decreased by the presence of the wall, with the ratio of the resonance frequency of a bubble at a distance d from a wall to the Minnaert frequency given by $(1+R_0/2d)^{-1/2}$, which equals 0.8 for a bubble in contact with the wall ($d = R_0$). This model has been extended, in particular, to account for propagation delays of sound waves between the bubble and the wall (Leighton 1994). However, it considers the bubble as a point source and is hence only valid for $d \gg R_0$.

Experiments have been conducted to characterize the change in bubble dynamics due to the proximity of a planar boundary, using optical tweezers to reposition the same bubble at increasing distances from the boundary (Garbin et al. 2007). Using this method, Helfield et al. (2014) measured the change in resonance frequency of the same bubble as a function of distance from a compliant agarose boundary. These authors found that such a soft wall has a weak effect on both resonance frequency and amplitude at resonance: These quantities showed relative variations within 10% when d was varied (**Figure 5*a***). Besides resonance properties, it has been shown that small-amplitude oscillations are sufficient to cause nonspherical deformations of a bubble near a viscoelastic boundary (Vos et al. 2011) and that the oscillations can cause the propagation of surface elastic waves on a viscoelastic half-space, with characteristics that depend on the viscoelastic properties of the material (Tinguely et al. 2016).

Theoretical models that take into account the effect of the compliance of the boundary on the bubble dynamics predict a shift in resonance frequency (Doinikov et al. 2011, Hay et al. 2012) and a change in nonlinear response (Doinikov & Bouakaz 2013). However, the models currently available predict resonance frequency shifts in opposite directions for interfaces with the same mechanical properties. These discrepancies, together with the scarcity of available experimental data, call for a better fundamental understanding of the interaction of oscillating bubbles with soft, deformable boundaries.

For the case of bubble collapse near deformable boundaries, experiments have shown that there is a strong qualitative effect of the elasticity of the boundary. The liquid jet formed during bubble collapse is always directed toward a hard boundary and away from a free surface. For soft boundaries, there is a threshold in elastic modulus below which the jet is directed away from the boundary. The example in **Figure 5*b*** is for a polyacrylamide layer. Numerical simulations of bubble collapse near an elastic boundary successfully predict jet reversal as a function of the elastic properties and the deformation of the boundary (Ohl et al. 2009).

Building on the theory for a single boundary or plate, models have also been proposed for bubbles between two plates (Hay et al. 2012, Doinikov & Bouakaz 2013) as a first step for approximating confinement conditions relevant to biomedical settings, which are covered next.

4.2. Bubbles in a Compliant Tube

Studying bubbles in a compliant tube is interesting for understanding the behavior of bubbles in blood vessels, which can be either beneficial for imaging and drug delivery (through sonoporation mechanisms) or detrimental, owing to the risks of blood vessel disruption.

Oğuz & Prosperetti (1998) considered bubbles in infinitely hard tubes. They showed that the natural frequencies of bubbles tend to be smaller than the Minnaert frequency. Indeed, because of the tube confinement, an oscillating bubble tends to put into motion all the liquid within the tube, which has a larger effective mass than the water put into motion around a bubble oscillating spherically in an unbounded medium. In addition to a numerical calculation, Oğuz & Prosperetti (1998) presented an insightful toy model when the bubble is confined enough to act as a piston across the tube. Sassaroli & Hynynen (2004) later considered theoretically the linear oscillations of bubbles in blood capillaries, similarly assumed to be rigid tubes.

Qin & Ferrara (2007) studied numerically the natural frequencies of bubbles in rigid and compliant vessels. In the latter case, they used a phenomenological relationship between the vessel deformation and the pressure difference across the vessel wall. They showed that while for rigid vessels, the natural frequency is below the Minnaert frequency and increases at increasing vessel radius, the result is exactly the opposite for compliant tubes; consistent with this result, they showed that the natural frequency is a decreasing function of the tube rigidity.

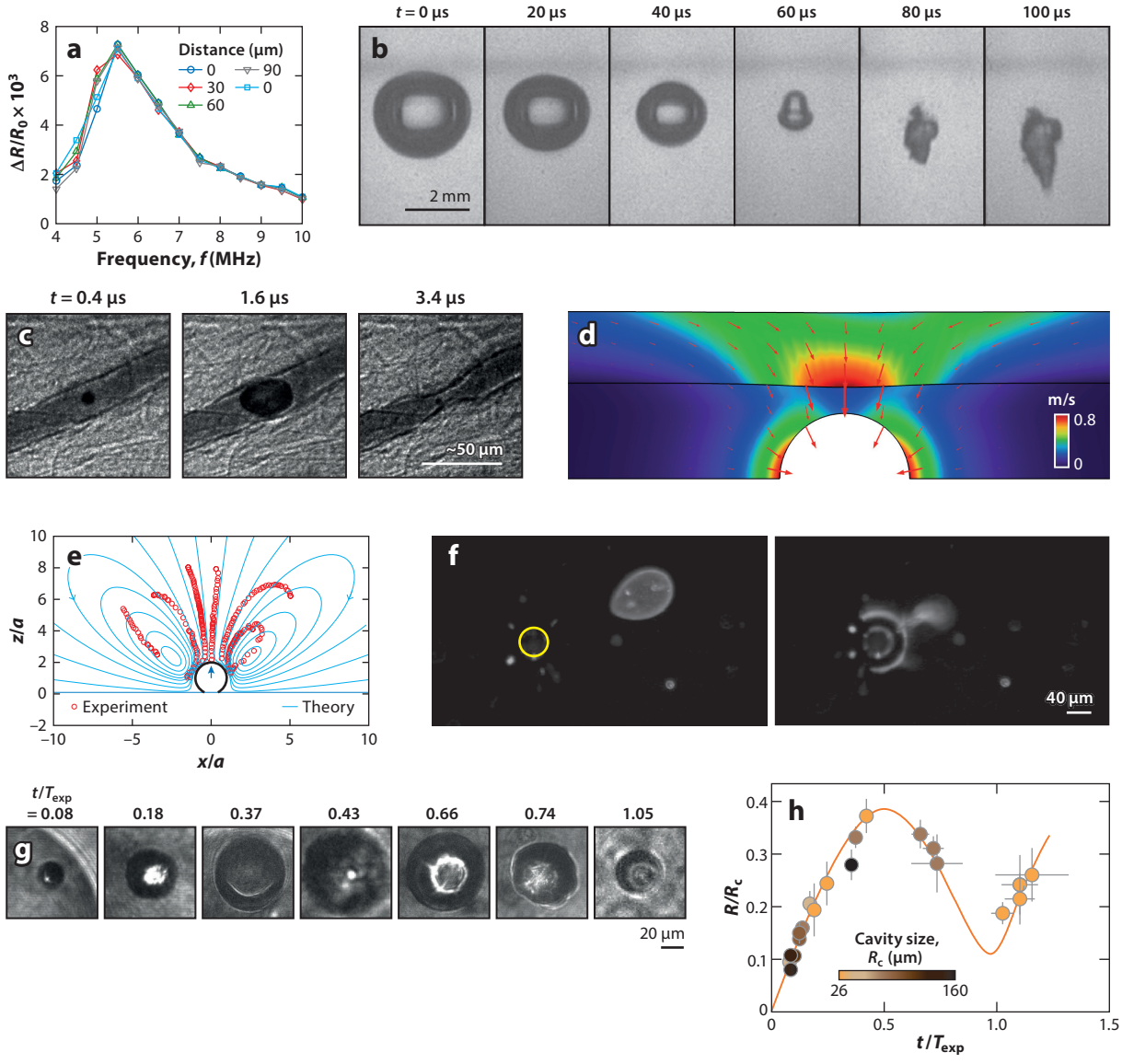

Figure 5

Bubble dynamics in the presence of soft confinement. (*a*) Resonance curve of a lipid-coated bubble at various controlled distances from a soft wall made of agarose gel. (*b*) Collapse of a laser-induced bubble near a polyacrylamide layer. (*c*) Snapshots of a bubble expanding and collapsing in a blood vessel, showing a strong invagination of the vessel upon bubble collapse. (*d*) Velocity field in the fluid and in the viscoelastic wall of a microvessel during bubble compression. (*e*) Acoustic streaming around a bubble in contact with a wall (*side view*). (*f*) Attraction and breakup of a vesicle in the streaming flow around a bubble (*top view*). (*g*) Strobe photography of bubble nucleation in confinement. T_{exp} is of the order of a microsecond. (*h*) Evolution of the radius after nucleation. Panels adapted with permission from (*a*) Helfield et al. (2014), copyright IOP Publishing; (*b*) Brujan et al. (2001); (*c*) Chen et al. (2011), copyright American Physical Society; (*d*) Chen et al. (2016), copyright Elsevier; (*e*,*f*) Marmottant & Hilgenfeldt (2003); and (*g*,*h*) Vincent et al. (2014), copyright Royal Society of Chemistry.

Martynov et al. (2009) proposed a theory of bubbles oscillating in elastic vessels. These authors used a simplified version of the model by Qin & Ferrara (2007) and extended the toy model of Oğuz & Prosperetti (1998) by including a finite vessel rigidity. They quantified the relative effect of the compressibility of the gas within the bubble (with bulk modulus of order p_0) and the compliance of the vessel; denoting by R_v and d_v the radius and thickness of the vessel wall, respectively, and E_v its shear modulus, they showed that the limit of a rigid vessel (Oğuz & Prosperetti 1998) corresponds to $E_v d_v / p_0 R_v \gg 1$, while a compliant vessel corresponds to $E_v d_v / p_0 R_v \ll 1$. In the latter case, they showed that the natural frequency is larger than the Minnaert frequency, in agreement with their simulations and those of Qin & Ferrara (2007), which they thus helped to rationalize.

Caskey et al. (2006) and Thomas et al. (2013) studied experimentally coated bubbles in rigid capillaries in vitro. They showed that increasing confinement led to a significant reduction of bubble oscillations. They did not observe a significant influence on the resonance frequency. Caskey et al. (2007) and Chen et al. (2011) presented ex vivo observations of microbubble response to ultrasound when confined in a blood vessel. Caskey et al. (2007) showed that bubble oscillation is strongly reduced when confined in a blood vessel, and Chen et al. (2011) showed that the bubble generates in general a stronger invagination than a distension of the neighboring blood vessel (**Figure 5*c***) and that, when collapsing, it generates a jet directed away from the blood vessel, consistent with other studies of bubble–soft wall interactions (Brujan et al. 2001). This work motivated numerical studies; for instance, Hosseinkhah et al. (2013) showed that invagination is the phase in which the maximum wall shear stress is created on an elastic vessel. **Figure 5*d*** shows the computed velocity field in the fluid and in the wall of a viscoelastic vessel during bubble compression (Chen et al. 2016).

4.3. Bubbles Near Suspended Cells or Vesicles

Acoustically driven bubbles can interact with small suspended bodies, such as cells or biomimetic vesicles, in a variety of geometries of biological, biomedical, and industrial relevance. For instance, ultrasound contrast agent microbubbles interact with blood cells in the vasculature, and cavitation bubbles interact with suspended microorganisms in bioreactors. Given its importance in a wealth of applications, a large body of work has addressed the effect of ultrasound on cell suspensions. A majority of these studies have used indirect experimental observations, which provide limited information on the bubble dynamics and bubble–cell interactions responsible for the observed phenomena. In this review, we limit the scope to recent studies that have provided direct, time-resolved visualizations of the interactions between bubbles and suspended cells or vesicles.

Le Gac et al. (2007) studied the interaction of a laser-induced cavitation bubble with suspended mammalian cells in microfluidic confinement. It was found that the cell membrane was damaged for cells located in the close vicinity of the collapsing bubble, while cells at a few bubble radii away were unaffected. Bacteria and yeast cells, which have thick cell walls, were also successfully damaged by cavitation bubbles in microfluidics (Tandiono et al. 2012). Zinin & Allen (2009) developed a theoretical model for the deformation of bacteria in the acoustic field generated by an oscillating bubble. They obtained the frequency of maximum area deformation of the bacteria, $\omega_K \sim \sqrt{K_A/\rho a^3}$, where K_A is the area stretching elasticity of the cell wall and a is the radius of the cell, suggesting that there is an optimal frequency of bubble oscillations that causes cell disruption.

Marmottant & Hilgenfeldt (2003) performed experiments showing that linear bubble oscillations are sufficient to rupture lipid vesicles. The microbubbles adhered to a solid surface and, upon excitation in ultrasound, generated a microstreaming flow (see **Figure 5*e***) that entrained suspended vesicles. When a vesicle reached the region of maximum strain rate, close to the bubble, the lipid bilayer was deformed to the point that it ruptured (see **Figure 5*f***). The flow-induced

deformation of the vesicle can be described by a capillary number, $Ca_K = \eta a \dot{\varepsilon}_{\max}/K_A$, based on the stretching elasticity of the lipid bilayer, K_A, where a is the vesicle radius and $\dot{\varepsilon}_{\max}$ is the maximum strain rate in the flow. This model for vesicle deformation, introduced by Marmottant et al. (2008), predicts a threshold value of the capillary number for vesicle rupture,

$$Ca_K^c = \sqrt{\frac{6}{5}}\frac{\sigma_c}{K_A}\sqrt{\frac{\Delta}{4\pi} + \frac{\sigma_c}{K_A}}, \qquad 14.$$

which depends on the vesicle excess area Δ and the lipid bilayer mechanical properties, K_A and σ_c, where σ_c is the rupture tension. Building on this theory, Pommella et al. (2015) performed experiments using vesicles with controlled membrane properties obtained by tuning the lipid composition and showed that selective vesicle rupture with respect to the membrane stretching elasticity can be obtained.

4.4. Bubbles in a Liquid-Filled Elastic Cavity

An extreme confinement situation is when a bubble occurs in a liquid-filled cavity, the bubble being confined by walls in all directions of space. This liquid cavity is itself framed within an elastic material and thus is compressed or dilated by bubble oscillations. The pressure away from the bubble (p_∞, as defined in Section 2.1) now depends on the bubble radius. Examples of such liquid cavities are found in trees, where ascending water is transported in tiny conduits, a few tens of micrometers in diameter and millimetric in length, within the xylem tissues (Tyree & Sperry 1989). The pressure of ascending water is negative because of evapotranspiration at the top of the tree, and cavitation can occur with the nucleation of bubbles. These bubbles are the source of an embolism whose growth proves to be fatal for a tree. Another astonishing example is the ejection mechanism of spores in ferns, which relies on cavitation bubbles occurring in a series of liquid-filled cavities located all along the arm of a catapult (Noblin et al. 2012).

Biomimetic elastic and porous materials were recently designed to include such liquid cavities while sustaining the very large negative liquid pressures resulting from pervaporation (Wheeler & Stroock 2008). These materials prove useful for studying cavitation dynamics in soft-matter materials, while confined cavitation was mostly studied in rocks (Caupin & Herbert 2006).

The bubble dynamics is strongly affected by the confinement, since an oscillation of the bubble volume must compress the liquid around and deform the elastic solid. For instance, just after the nucleation, a cavitation bubble quickly grows and then oscillates around an equilibrium radius that relaxes the liquid pressure, with very large variations of the bubble volume. Natural frequencies of these oscillations are well above the Minnaert frequency (Vincent et al. 2012, Vincent & Marmottant 2017), reaching megahertz frequency for cavities of a few dozen micrometers in radius. The reason for such high-frequency oscillations lies in the fact that the effective stiffness resistance of the medium against oscillations is tremendously increased. The gas compression modulus (equal to κp_0) is indeed negligible in front of the liquid compression modulus ($K_l = 2.2$ GPa) and the solid shear modulus G. The natural oscillation of confined bubbles of radius R_0 in a cavity of radius R_c is

$$\omega_0^2 = \frac{3K}{\rho R_0^2}\left(\frac{R_0}{R_c}\right)^3, \qquad 15.$$

where K is an effective modulus given by $\frac{1}{K} = \frac{1}{K_l} + \frac{3}{4G}$ that describes the effective elastic response from the elasticity of water and solid, which act as springs in a series. This natural oscillation frequency is much higher than for a free bubble. For comparison, with the Minnaert frequency

(Equation 8), the denominator is the same as in Equation 15 but the numerator is much smaller—$3\gamma p_0$ instead of $3K(R_0/R_c)^3$.

5. CONCLUSIONS

Bubbles are simple but fascinating objects. They exhibit a strong ability to oscillate in response to sound, while being very sensitive to their surrounding environment. They prove to be useful probes of the viscoelastic properties of the medium or the presence of boundaries. The response of bubbles with a coating is strongly affected by the presence of the coating layer, which is either thick or a monolayer of molecules or particles. Bubbles display nonlinear effects that can be isolated by ultrasound echography, not only in their high-amplitude regime but also at small amplitude when there is strong coupling with the nonlinear rheology of the medium.

As a perspective, we expect a variety of promising developments in the future. We see three directions that seem especially fruitful in view of the recent literature. First, bubbles being active miniature tracers, they can probe the high-frequency rheology of soft and biological materials. One could imagine that such information would pave the way for 3D maps of the rheological properties of heterogeneous media, following bubbles navigating in different regions of these media. Second, further progress is expected in the description of the constitutive behavior of soft materials at high strain rate, thanks to the information obtained from experiments where oscillating or collapsing bubbles are used as rheological probes. In addition, the link between the microscopic changes in the material upon deformation and the macroscopic mechanical response remains to be explored. One example is the case of particle-coated bubbles, for which interfacial constitutive models are currently lacking. Last, the interaction of a compliant flat wall and oscillating bubbles deserves to be better understood, both to quantify the wall influence on bubble dynamics and as a starting point to control the physical and biological effects of bubbles on soft boundaries with more complex geometries, like blood vessels.

DISCLOSURE STATEMENT

The authors are not aware of any biases that might be perceived as affecting the objectivity of this review.

ACKNOWLEDGMENTS

We thank M. Böhmer, M.A. Borden, M. De Corato, A. Doinikov, D.E. Goertz, E. Johnsen, and C.-D. Ohl for helpful discussions. We thank D. Lohse and M. Versluis for introducing us to this topic and for their continued support. P.M. is supported by ERC Consolidator Grant 614655. V.G. is supported by ERC Starting Grant 639221.

LITERATURE CITED

Abkarian M, Subramaniam AB, Kim SH, Larsen RJ, Yang SM, Stone HA. 2007. Dissolution arrest and stability of particle-covered bubbles. *Phys. Rev. Lett.* 99:188301

Allen JS, Roy RA. 2000a. Dynamics of gas bubbles in viscoelastic fluids. I. Linear viscoelasticity. *J. Acoust. Soc. Am.* 107:3167–78

Allen JS, Roy RA. 2000b. Dynamics of gas bubbles in viscoelastic fluids. II. Nonlinear viscoelasticity. *J. Acoust. Soc. Am.* 108:1640–50

Asaki TJ, Marston PL. 1997. The effects of a soluble surfactant on quadrupole shape oscillations and dissolution of air bubbles in water. *J. Acoust. Soc. Am.* 102:3372–77

A model of bubble dynamics in a viscoelastic liquid using a linear constitutive equation (Maxwell model).

Asaki TJ, Thiessen DB, Marston PL. 1995. Effect of an insoluble surfactant on capillary oscillations of bubbles in water: observation of a maximum in the damping. *Phys. Rev. Lett.* 75:2686–89

Blake JR, Gibson DC. 1987. Cavitation bubbles near boundaries. *Annu. Rev. Fluid Mech.* 19:99–123

Böhmer M, Schroeders R, Steenbakkers JAM, de Winter SHPM, Duineveld PA, et al. 2006. Preparation of monodisperse polymer particles and capsules by ink-jet printing. *Colloids Surf. A* 289:96–104

Borden MA, Longo ML. 2002. Dissolution behavior of lipid monolayer-coated, air-filled microbubbles: effect of lipid hydrophobic chain length. *Langmuir* 18:9225–33

Brujan EA. 2010. *Cavitation in Non-Newtonian Fluids: With Biomedical and Bioengineering Applications*. Berlin: Springer-Verlag

Brujan EA, Nahen K, Schmidt P, Vogel A. 2001. Dynamics of laser-induced cavitation bubbles near elastic boundaries: influence of the elastic modulus. *J. Fluid Mech.* 433:283–314

An experimental study of bubble collapse near a soft boundary showing jet reversal below a threshold in elastic modulus.

Brujan EA, Vogel A. 2006. Stress wave emission and cavitation bubble dynamics by nanosecond optical breakdown in a tissue phantom. *J. Fluid Mech.* 558:281–308

Caskey CF, Kruse DE, Dayton PA, Kitano TK, Ferrara KW. 2006. Microbubble oscillation in tubes with diameters of 12, 25, and 195 microns. *Appl. Phys. Lett.* 88:033902

Caskey CF, Stieger SM, Qin S, Dayton PA, Ferrara KW. 2007. Direct observations of ultrasound microbubble contrast agent interaction with the microvessel wall. *J. Acoust. Soc. Am.* 122:1191–200

Caupin F, Herbert E. 2006. Cavitation in water: a review. *C. R. Phys.* 7:1000–17

Cavalieri F, Ashokkumar M, Grieser F, Caruso F. 2008. Ultrasonic synthesis of stable, functional lysozyme microbubbles. *Langmuir* 24:10078–83

Chatterjee D, Sarkar K. 2003. A Newtonian rheological model for the interface of microbubble contrast agents. *Ultrasound Med. Biol.* 29:1749–57

Chen C, Gu Y, Tu J, Guo X, Zhang D. 2016. Microbubble oscillating in a microvessel filled with viscous fluid: a finite element modeling study. *Ultrasonics* 66:54–64

Chen DT, Wen Q, Janmey PA, Crocker JC, Yodh AG. 2010. Rheology of soft materials. *Annu. Rev. Condens. Matter Phys.* 1:301–22

Chen H, Kreider W, Brayman AA, Bailey MR, Matula TJ. 2011. Blood vessel deformations on microsecond time scales by ultrasonic cavitation. *Phys. Rev. Lett.* 106:034301

A time-resolved visualization of blood vessel deformation during bubble collapse in an ex vivo experiment.

Choi JJ, Selert K, Vlachos F, Wong A, Konofagou EE. 2011. Noninvasive and localized neuronal delivery using short ultrasonic pulses and microbubbles. *PNAS* 108:16539–44

Church CC. 1995. The effects of an elastic solid surface layer on the radial pulsations of gas bubbles. *J. Acoust. Soc. Am.* 97:1510–21

Coussios CC, Roy RA. 2008. Applications of acoustics and cavitation to noninvasive therapy and drug delivery. *Annu. Rev. Fluid Mech.* 40:395–420

de Jong N, Hoff L, Skotland T, Bom N. 1992. Absorption and scatter of encapsulated gas filled microspheres: theoretical considerations and some measurements. *Ultrasonics* 30:95–103

Doinikov AA, Aired L, Bouakaz A. 2011. Acoustic scattering from a contrast agent microbubble near an elastic wall of finite thickness. *Phys. Med. Biol.* 56:6951–67

A theoretical model for the dynamics of a bubble near an elastic wall of arbitrary thickness.

Doinikov AA, Bouakaz A. 2011. Review of shell models for contrast agent microbubbles. *IEEE Trans. Ultrason. Ferroelec. Freq. Control* 58:981–93

Doinikov AA, Bouakaz A. 2013. Ultrasonically induced dynamics of a contrast agent microbubble between two parallel elastic walls. *Phys. Med. Biol.* 58:6797–814

Doinikov AA, Dayton PA. 2007. Maxwell rheological model for lipid-shelled ultrasound microbubble contrast agents. *J. Acoust. Soc. Am.* 121:3331–40

Dollet B, van der Meer SM, Garbin V, de Jong N, Lohse D, Versluis M. 2008. Nonspherical oscillations of ultrasound contrast agent microbubbles. *Ultrasound Med. Biol.* 34:1465–73

Edwards DA, Brenner H, Wasan DT, eds. 1991. *Interfacial Transport Processes and Rheology*. Boston: Butterworth-Heinemann

Emmer M, van Wamel A, Goertz DE, de Jong N. 2007. The onset of microbubble vibration. *Ultrasound Med. Biol.* 33:941–49

Estrada JB, Barajas C, Henann DL, Johnsen E, Franck C. 2018. High strain-rate soft material characterization via inertial cavitation. *J. Mech. Phys. Solids* 112:291–317

Everitt S, Harlen O, Wilson H, Read D. 2003. Bubble dynamics in viscoelastic fluids with application to reacting and non-reacting polymer foams. *J. Non-Newton. Fluid Mech.* 114:83–107
Faez T, Emmer M, Kooiman K, Versluis M, van der Steen AFW, de Jong N. 2013. 20 years of ultrasound contrast agent modeling. *IEEE Trans. Ultrason. Ferroelec. Freq. Control* 60:7–20
Fogler HS, Goddard JD. 1970. Collapse of spherical cavities in viscoelastic fluids. *Phys. Fluids* 13:1135–41
Frinking PJA, de Jong N. 1998. Acoustic modeling of shell-encapsulated gas bubbles. *Ultrasound Med. Biol.* 24:523–33
Fujii S, Nakamura Y. 2017. Stimuli-responsive bubbles and foams stabilized with solid particles. *Langmuir* 33:7365–79
Gao Y, Chan CU, Gu Q, Lin X, Zhang W, et al. 2016. Controlled nanoparticle release from stable magnetic microbubble oscillations. *NPG Asia Mater.* 8:e260
Garbin V, Cojoc D, Ferrari E, Di Fabrizio E, Overvelde M, et al. 2007. Changes in microbubble dynamics near a boundary revealed by combined optical micromanipulation and high-speed imaging. *Appl. Phys. Lett.* 90:114103
Gaudron R, Warnez M, Johnsen E. 2015. Bubble dynamics in a viscoelastic medium with nonlinear elasticity. *J. Fluid Mech.* 766:54–75
Gorce JM, Arditi M, Schneider M. 2000. Influence of bubble size distribution on the echogenicity of ultrasound contrast agents: a study of SonoVue^{TM}. *Investig. Radiol.* 35:661–71
Hamaguchi F, Ando K. 2015. Linear oscillation of gas bubbles in a viscoelastic material under ultrasound irradiation. *Phys. Fluids* 27:113103
Hay TA, Ilinskii YA, Zabolotskaya EA, Hamilton MF. 2012. Model for bubble pulsation in liquid between parallel viscoelastic layers. *J. Acoust. Soc. Am.* 132:124–37
Helfield BL, Leung BY, Goertz DE. 2014. The effect of boundary proximity on the response of individual ultrasound contrast agent microbubbles. *Phys. Med. Biol.* 59:1721–45
Hoff L, Sontum PC, Hovem JM. 2000. Oscillations of polymeric microbubbles: effect of the encapsulating shell. *J. Acoust. Soc. Am.* 107:2272–80
Hosseinkhah N, Chen H, Matula TJ, Burns PN, Hynynen K. 2013. Mechanisms of microbubble–vessel interactions and induced stresses: a numerical study. *J. Acoust. Soc. Am.* 134:1875–85
Hua C, Johnsen E. 2013. Nonlinear oscillations following the Rayleigh collapse of a gas bubble in a linear viscoelastic (tissue-like) medium. *Phys. Fluids* 25:083101
Ichihara M. 2008. Dynamics of a spherical viscoelastic shell: implications to a criterion for fragmentation/expansion of bubbly magma. *Earth Planet. Sci. Lett.* 265:18–32
Jamburidze A, De Corato M, Huerre A, Pommella A, Garbin V. 2017. High-frequency linear rheology of hydrogels probed by ultrasound-driven microbubble dynamics. *Soft Matter* 13:3946–53
Jiménez-Fernández J, Crespo A. 2005. Bubble oscillation and inertial cavitation in viscoelastic fluids. *Ultrasonics* 43:643–51
Kawchuk GN, Fryer J, Jaremko JL, Zeng H, Rowe L, Thompson R. 2015. Real-time visualization of joint cavitation. *PLOS ONE* 10:e0119470
Keller JB, Miksis M. 1980. Bubble oscillations of large amplitude. *J. Acoust. Soc. Am.* 68:628–33
Krasovitski B, Frenkel V, Shoham S, Kimmel E. 2011. Intramembrane cavitation as a unifying mechanism for ultrasound-induced bioeffects. *PNAS* 108:3258–63
Kundu S, Crosby AJ. 2009. Cavitation and fracture behavior of polyacrylamide hydrogels. *Soft Matter* 5:3963–68
Langevin D. 2014. Rheology of adsorbed surfactant monolayers at fluid surfaces. *Annu. Rev. Fluid Mech.* 46:47–65
Le Gac S, Zwaan E, van den Berg A, Ohl CD. 2007. Sonoporation of suspension cells with a single cavitation bubble in a microfluidic confinement. *Lab Chip* 7:1666–72
Leighton TG. 1994. *The Acoustic Bubble*. London: Academic
Liu Y, Sugiyama K, Takagi S, Matsumoto Y. 2012. Surface instability of an encapsulated bubble induced by an ultrasonic pressure wave. *J. Fluid Mech.* 691:315–40
Lotsberg O, Hovem JM, Aksum B. 1996. Experimental observations of subharmonic oscillations in Infoson bubbles. *J. Acoust. Soc. Am.* 99:1366–69

Luan Y, Lajoinie G, Gelderblow E, Skachkov I, van der Steen AFW, et al. 2014. Lipid shedding from single oscillating microbubbles. *Ultrasound Med. Biol.* 40:1834–46

Lum JS, Dove JD, Murray TW, Borden MA. 2016. Single microbubble measurements of lipid monolayer viscoelastic properties for small-amplitude oscillations. *Langmuir* 32:9410–17

Macosko C. 1994. *Rheology: Principles, Measurements, and Applications*. New York: Wiley-VCH

Marmottant P, Biben T, Hilgenfeldt S. 2008. Deformation and rupture of lipid vesicles in the strong shear flow generated by ultrasound-driven microbubbles. *Proc. R. Soc. Lond. A* 464:1781–800

Marmottant P, Bouakaz A, de Jong N, Quilliet C. 2011. Buckling resistance of solid shell bubbles under ultrasound. *J. Acoust. Soc. Am.* 129:1231–39

Marmottant P, Hilgenfeldt S. 2003. Controlled vesicle deformation and lysis by single oscillating bubbles. *Nature* 423:153–56

Marmottant P, van der Meer S, Emmer M, Versluis M, de Jong N, et al. 2005. A model for large amplitude oscillations of coated bubbles accounting for buckling and rupture. *J. Acoust. Soc. Am.* 118:3499–505

Martynov S, Stride E, Saffari N. 2009. The natural frequencies of microbubble oscillation in elastic vessels. *J. Acoust. Soc. Am.* 126:2963–72

Morgan KE, Allen JS, Dayton PA, Chomas JE, Klibanov AL, Ferrara KW. 2000. Experimental and theoretical evaluation of microbubble behavior: effect of transmitted phase and bubble size. *IEEE Trans. Ultrason. Ferroelec. Freq. Control* 47:1494–509

Naude J, Méndez F. 2008. Periodic and chaotic acoustic oscillations of a bubble gas immersed in an upper convective maxwell fluid. *J. Non-Newton. Fluid Mech.* 155:30–38

Noblin X, Rojas N, Westbrook J, Llorens C, Argentina M, Dumais J. 2012. The fern sporangium: a unique catapult. *Science* 335:1322

Oğuz HN, Prosperetti A. 1998. The natural frequency of oscillation of gas bubbles in tubes. *J. Acoust. Soc. Am.* 103:3301–8

Ohl S, Klaseboer E, Khoo B. 2009. The dynamics of a non-equilibrium bubble near bio-materials. *Phys. Med. Biol.* 54:6313–36

Overvelde M, Garbin V, Sijl J, Dollet B, de Jong N, et al. 2010. Nonlinear shell behavior of phospholipid-coated microbubbles. *Ultrasound Med. Biol.* 36:2080–92

Pagani G, Green MJ, Poulin P, Pasquali M. 2012. Competing mechanisms and scaling laws for carbon nanotube scission by ultrasonication. *PNAS* 109:11599–604

Parrales MA, Fernández JM, Pérez-Saborid M, Kopechek JA, Porter TM. 2014. Acoustic characterization of monodisperse lipid-coated microbubbles: relationship between size and shell viscoelastic properties. *J. Acoust. Soc. Am.* 136:1077–84

Paul S, Katiyar A, Sarkar K, Chatterjee D, Shi WT, Forsberg F. 2010. Material characterization of the encapsulation of an ultrasound contrast agent microbubble and its subharmonic response: strain-softening interfacial model. *J. Acoust. Soc. Am.* 127:3846–57

Plesset MS, Prosperetti A. 1977. Bubble dynamics and cavitation. *Annu. Rev. Fluid Mech.* 9:145–85

Pommella A, Brooks NJ, Seddon JM, Garbin V. 2015. Selective flow-induced vesicle rupture to sort by membrane mechanical properties. *Sci. Rep.* 5:13163

Postema M, Marmottant P, Lancée CT, Hilgenfeldt S, de Jong N. 2004. Ultrasound-induced microbubble coalescence. *Ultrasound Med. Biol.* 30:1337–44

Poulichet V, Garbin V. 2015. Ultrafast desorption of colloidal particles from fluid interfaces. *PNAS* 112:5932–37

Poulichet V, Huerre A, Garbin V. 2017. Shape oscillations of particle-coated bubbles and directional particle expulsion. *Soft Matter* 13:125–33

Prosperetti A. 1974. Nonlinear oscillations of gas bubbles in liquids: steady-state solutions. *J. Acoust. Soc. Am.* 56:878–85

Prosperetti A. 1977. Thermal effects and damping mechanisms in the forced radial oscillations of gas bubbles in liquids. *J. Acoust. Soc. Am.* 61:17–27

Prosperetti A. 1982. A generalization of the Rayleigh–Plesset equation of bubble dynamics. *Phys. Fluids* 25:409–10

An analysis of freely decaying oscillations of coated bubbles to measure surface elasticity of lipid monolayers at strain rates of 10^6 s^{-1}.

Discovered "compression only" of oscillating coated bubbles and proposed a constitutive equation that accurately captures this behavior and other nonlinearities.

A theoretical model describing the coupling of the oscillations of a bubble with a surrounding compliant tube.

A comprehensive experimental study of the various manifestations of nonlinear oscillations of lipid-coated bubbles.

Prosperetti A. 2013. A general derivation of the subharmonic threshold for non-linear bubble oscillations. *J. Acoust. Soc. Am.* 133:3719–26

Qin S, Ferrara KW. 2007. The natural frequency of nonlinear oscillations of ultrasound contrast agents in microvessels. *Ultrasound Med. Biol.* 33:1140–48

Sarkar K, Shi WT, Chatterjee D, Forsberg F. 2005. Characterization of ultrasound contrast microbubbles using in vitro experiments and viscous and viscoelastic interface models for encapsulation. *J. Acoust. Soc. Am.* 118:539–50

Sassaroli E, Hynynen K. 2004. Forced linear oscillations of microbubbles in blood capillaries. *J. Acoust. Soc. Am.* 115:3235–43

Shankar PM, Krishna PD, Newhouse VL. 1998. Advantages of subharmonic over second harmonic backscatter for contrast-to-tissue echo enhancement. *Ultrasound Med. Biol.* 24:395–99

Shankar PM, Krishna PD, Newhouse VL. 1999. Subharmonic backscattering from ultrasound contrast agents. *J. Acoust. Soc. Am.* 106:2104–10

Sijl J, Dollet B, Overvelde M, Garbin V, Rozendal T, et al. 2010. Subharmonic behavior of phospholipid-coated ultrasound contrast agent microbubbles. *J. Acoust. Soc. Am.* 128:3239–52

Strasberg M. 1953. The pulsation frequency of nonspherical gas bubbles in liquids. *J. Acoust. Soc. Am.* 25:536–37

Stride E. 2008. The influence of surface adsorption on microbubble dynamics. *Philos. Trans. R. Soc. A* 366:2103–15

Stride E, Pancholi K, Edirisinghe M, Samarasinghe S. 2008. Increasing the nonlinear character of microbubble oscillations at low acoustic pressures. *J. R. Soc. Interface* 5:807–11

Strybulevych A, Leroy V, Scanlon MG, Page JH. 2009. Acoustic microrheology: shear moduli of soft materials determined from single bubble oscillations. In *Proceedings of Symposium on Ultrasonic Electronics*, Vol. 30, pp. 395–96. **http://www.use-jp.org/USE2010/proceedings/USE09/pdf/2E1-2.pdf**

Sun Y, Kruse DE, Dayton PA, Ferrara KW. 2005. High-frequency dynamics of ultrasound contrast agents. *IEEE Trans. Ultrason. Ferroelec. Freq. Control* 52:1981–91

Tandiono T, Ow DS, Driessen L, Chin CS, Klaseboer E, et al. 2012. Sonolysis of *Escherichia coli* and *Pichia pastoris* in microfluidics. *Lab Chip* 12:780–86

Thomas DH, Sboros V, Emmer M, Vos H, de Jong N. 2013. Microbubble oscillations in capillary tubes. *IEEE Trans. Ultrason. Ferroelec. Freq. Control* 60:105–14

Tinguely M, Hennessy MG, Pommella A, Matar OK, Garbin V. 2016. Surface waves on a soft viscoelastic layer produced by an oscillating microbubble. *Soft Matter* 12:4247–56

Tsiglifis K, Pelekasis NA. 2008. Nonlinear radial oscillations of encapsulated microbubbles subject to ultrasound: the effect of membrane constitutive law. *J. Acoust. Soc. Am.* 123:4059–70

Tsiglifis K, Pelekasis NA. 2011. Parametric stability and dynamic buckling of an encapsulated microbubble subject to acoustic disturbances. *Phys. Fluids* 23:012102

Tu J, Guan J, Qiu Y, Matula TJ. 2009. Estimating the shell parameters of SonoVue® microbubbles using light scattering. *J. Acoust. Soc. Am.* 126:2954–62

Tyree M, Sperry J. 1989. Vulnerability of xylem to cavitation and embolism. *Annu. Rev. Plant Physiol. Mol. Biol.* 40:19–36

van der Meer SM, Dollet B, Voormolen MM, Chin CT, Bouakaz A, et al. 2007. Microbubble spectroscopy of ultrasound contrast agents. *J. Acoust. Soc. Am.* 121:648–56

van Rooij T, Luan Y, Renaud G, van der Steen AFW, Versluis M, et al. 2015. Non-linear response and viscoelastic properties of lipid-coated microbubbles: DSPC versus DPPC. *Ultrasound Med. Biol.* 41:1432–45

Versluis M. 2013. High-speed imaging in fluids. *Exp. Fluids* 54:1–35

Versluis M, Goertz DE, Palanchon P, Heitman IL, van der Meer SM, et al. 2010. Microbubble shape oscillations excited through ultrasonic parametric driving. *Phys. Rev. E* 82:026321

Vincent O, Marmottant P. 2017. On the statics and dynamics of fully confined bubbles. *J. Fluid Mech.* 827:194–224

Vincent O, Marmottant P, Gonzalez-Avila SR, Ando K, Ohl C-D. 2014. The fast dynamics of cavitation bubbles within water conned in elastic solids. *Soft Matter* 10:1455–61

Vincent O, Marmottant P, Quinto-Su PA, Ohl CD. 2012. Birth and growth of cavitation bubbles within water under tension confined in a simple synthetic tree. *Phys. Rev. Lett.* 108:184502

Vos H, Dollet B, Versluis M, de Jong N. 2011. Nonspherical shape oscillations of coated microbubbles in contact with a wall. *Ultrasound Med. Biol.* 37:935–48

Warnez MT, Johnsen E. 2015. Numerical modeling of bubble dynamics in viscoelastic media with relaxation. *Phys. Fluids* 27:063103

Wheeler TD, Stroock AD. 2008. The transpiration of water at negative pressures in a synthetic tree. *Nature* 455:208–12

Yang X, Church CC. 2005. A model for the dynamics of gas bubbles in soft tissue. *J. Acoust. Soc. Am.* 118:3595–606

Zhao X, Quinto-Su PA, Ohl CD. 2009. Dynamics of magnetic bubbles in acoustic and magnetic fields. *Phys. Rev. Lett.* 102:024501

Zimberlin JA, Sanabria-DeLong N, Tew GN, Crosby AJ. 2007. Cavitation rheology for soft materials. *Soft Matter* 3:763–67

Zinin PV, Allen JS. 2009. Deformation of biological cells in the acoustic field of an oscillating bubble. *Phys. Rev. E* 79:021910

A model of bubble dynamics in a viscoelastic medium using a highly general constitutive equation for the linear and nonlinear cases.

A model of bubble dynamics in a viscoelastic solid using a linear constitutive equation (Kelvin–Voigt model).

Annual Review of Fluid Mechanics

Volume 51, 2019

Contents

Indexes

Errata

An online log of corrections to *Annual Review of Fluid Mechanics* articles may be found at http://www.annualreviews.org/errata/fluid